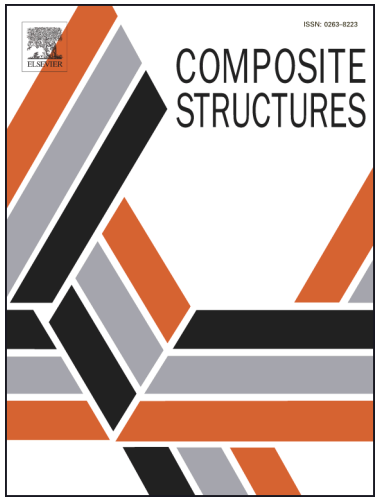


# Guided Waves in A Composite Winglet Structure: Numerical and Experimental Investigations

A. De Luca, D. Perfetto, A. De Fenza, G. Petrone, F. Caputo

PII: S0263-8223(18)32058-0
DOI: https://doi.org/10.1016/j.compstruct.2018.11.048
Reference: COST 10413

To appear in: *Composite Structures*

Received Date: 5 June 2018
Revised Date: 9 November 2018
Accepted Date: 16 November 2018

Please cite this article as: De Luca, A., Perfetto, D., De Fenza, A., Petrone, G., Caputo, F., Guided Waves in A Composite Winglet Structure: Numerical and Experimental Investigations, *Composite Structures* (2018), doi: https://doi.org/10.1016/j.compstruct.2018.11.048

# GUIDED WAVES IN A COMPOSITE WINGLET STRUCTURE: NUMERICAL AND EXPERIMENTAL INVESTIGATIONS

A. De Luca[1]*, D. Perfetto[1], A. De Fenza[2], G. Petrone[2], F. Caputo[1]

[1] Department of Engineering, University of Campania "L. Vanvitelli", Via Roma 29, 81031 Aversa, Italy.

[2]Department of Industrial Engineering – Aerospace Division, Università degli Studi di Napoli "Federico II", Via Claudio 21, 80125, Napoli, Italy

*Corresponding author. Tel.: +39 0815010318
E-mail address: alessandro.deluca@unicampania.it

**Keywords**: Composite; Winglet; Experimental investigations; Guided waves; Lamb waves; FE analysis.

## Abstract

The paper deals with numerical and experimental investigations aimed to develop a Finite Element (FE) model for predicting wave propagation in a blended composite winglet. Material anisotropy, inhomogeneity, multi-layered configuration and complex geometries tend to increase the complexity of the wave propagation phenomena and consequently the development of established FE models. Moreover, even if 2D finite elements seem to be not appropriate for modelling guided waves propagation, especially for complex anisotropic structural components, they are more attractive than 3D ones, because of the computational cost saving. For this reason, part of the presented research activity is addressed to investigate the efficiency of shell finite elements in modelling guided waves propagation in a such complex structure as a winglet. The development of an efficient model depends also on the numerical characterization of the medium within which guided waves propagate through. As a consequence, preliminary simple experimental bending and modal tests have been carried out to support the material properties modelling. Subsequently, guided wave propagation FE analyses were performed and the results compared with provided experimental data. A good agreement between numerical and experimental results of the different analyses has been achieved in terms of both signal time of flight and amplitudes.

## 1 Introduction

Guided Lamb waves are widely acknowledged as one of the most encouraging tools for quantitative identification of damages in composite structures and relevant researches were intensively conducted since 1980. They were discovered by Horace Lamb in 1917 [1], as waves propagating in thin plates, and only in 1950 it was formulated a comprehensive theory by Mindlin; experimental work on the same topic were conducted by Schoch in 1952 [2] and Frederick in 1962 [3]. Only in 1961, thanks to Worlton [4], Lamb waves were introduced for the first time as a tool for damage detection, establishing their fundamental use as a prominent non-destructive evaluation tool.
Due to their high susceptibility to interferences caused by discontinuities on the propagation path (e.g. in case of damage or boundary edge) and their ability to travel over a long distance with a low

power consumption, Lamb waves allow quickly inspecting and monitoring a broad area, even in materials characterized by a high attenuation ratio, such as Glass Fibre Reinforced Polymers (GFRP). In particular, the ability to examine the entire cross-sectional area of the structure, by selecting the proper wave modes, allows detecting both internal and surface damages/defects.

The potential damage types that a Lamb wave-based system can detect are summarized by Rose [5]. A Lamb wave-based identification, associated with a damage detection method, provides useful information such as qualitative indication of the occurrence of damage [6-7], quantitative assessment of the position of damage [8-10] and quantitative estimation of its severity; all this information can contribute significantly to the prediction of the residual service life of the component [11]. However, the monitoring of the structural health and the propagation of guided waves in complex structures, such as the winglet proposed in this article, is notoriously very complex [12]. With very high speed, waves reflected from boundaries may easily conceal damage-scattered components in the signals. In the same way, the different layup for upper and lower winglet surfaces, as well as the foam in the internal region, the spar stiffener and the double-curvature skin could induce variations in wave propagation. For these reasons, in order to better understand the physical principles of guided wave propagation within complex structures, numerical simulations are essential. The capability to faithfully reproduce what happens during experiments through numerical simulations could be the key issue in developing innovative diagnostic and prognostic techniques for Structural Health Monitoring (SHM) applications [13].

The wave propagation in plate can be modelled by solving the equation of motion analytically, semi-analytically and numerically [14]. The former two methods, however, have limited applications, especially when the investigations involve complex and large real engineering structures [15], as the investigated winglet [12]. The latter, such as the FE one [16-19], can give a significant contribution to the prediction and the understanding of the wave propagation mechanisms. In this paper, the FE method has been used to carry out the numerical investigations.

The validity and the efficiency of a FE model aimed to such purpose strictly depend on the choice of the finite element type as well as on its characteristic length. Concerning the characteristic length, it depends on the wave modes to be modelled. For the first symmetric, $S_0$, and antisymmetric, $A_0$, modes it should be set in such a way to achieve at least 10 nodes per wavelength (NPW) [15]. High value of NPW is needed to model higher waves modes [15, 20]. Concerning the element type, several authors investigated the use of both two-dimensional and three-dimensional approaches. Yang et al. [21] modelled isotropic and quasi-isotropic composite laminates using brick and continuum shell elements. Sharif-Khodaei et al. [20] investigated the best finite element type for the modelling of Lamb wave propagation in aluminium and CFRP plates, by proving that 2D (shell and continuum shell) and 3D finite elements work properly for the prediction of the first wave modes. Such investigations are very reliable if focused on simple plates; complex geometry and strong curvatures may lower the prediction capability of the FE model.

This paper aims to develop a 2D (shell based) FE model for the simulation of guided wave propagation in a such complex anisotropic structural component as the aforementioned winglet, which was previously investigated by experiment in [12].

2D finite elements are more attractive respect to 3D ones, since the computational costs saving. For this reason, in this paper, a preliminary stage is addressed to investigate the efficiency of shell finite elements against solid ones in modelling guided waves in a such complex structure as the winglet.

Specifically, under this purpose, two FE models based on 2D and 3D finite elements respectively have been developed and the results compared. All analyses have been performed by means of Abaqus® 6.14 code. Also a mesh sensitivity analysis has been carried out to set the appropriate finite element characteristic length.

Moreover, in order to numerically characterize, as best as possible, the medium which guided waves propagate through, before starting with guided waves simulation the accuracy of the material modelling has been assessed by simulating two simpler experimental tests (bending and modal ones), as widely described in [12].

Concerning guided waves simulation, the correlation between numerical and experimental results has been carried out by comparing the signals recorded at the sensors with the predicted ones, by extracting and comparing Time-of-Flight (ToF) features.

## 2 Experimental investigations

Material inhomogeneity, anisotropy, properties uncertainty and multi-layered configuration characterizing the investigated winglet can lead to several difficulties during numerical modelling [22], therefore the first step for the development of an efficient model is to numerically characterize, as best as possible, the medium which guided waves propagate through. In order to do this, the research strategy consisted in the execution of preliminary simple experimental tests to support the development of the FE model and the characterization of the medium material properties.
Bending and modal tests have been performed to assess the efficiency of the FE model in simulating the winglet behaviour under different loading conditions.
A preliminary test article description is proposed in Section 2.1; the static test (bending) is described in Section 2.2 while the modal analysis is illustrated in Section 2.3; finally, the experimental set-up arranged for guided wave propagation is presented and discussed in Section 2.4.

### 2.1 Test article

The geometrical complexity due to the double curvature of the skin, the different layups for upper and lower winglet surfaces, as well as the foam in the internal region and the spar stiffener, imply that the winglet is manufactured as two single shell parts joined together (Figure 1.a). The winglet is composed by fabric laminate in fiberglass fibres infused with epoxy resin and foam coring. The spar stiffener and the laminate core, made of high-performance low-density foam (Figure 1.b), give high contribution to the static and dynamic strength of the winglet. In Table 1 the mechanical properties of the lamina are listed; the different lay-ups are listed in Table 2, while Figure 2 shows the upper and lower parts, each one with the respective assigned materials (colours in Table 2 are associated to areas in Figure 2).

Figure 1 - Winglet (a); particular on the spar junction (b) [12].

Table 1 - Lamina material properties [12].

| Material properties | Symbol | Units | Foam | Fiberglass |
|---|---|---|---|---|
| Young modulus | E | [GPa] | 1.3 | - |
| Longitudinal Young modulus | $E_1$ | [GPa] | - | 11 |
| Transversal Young modulus | $E_2$ | [GPa] | - | 6.5 |
| Shear modulus | G | [GPa] | 0.303 | - |
| Shear modulus | $G_{12}$ | [GPa] | - | 4.0 |
| Poisson's ratio | ν | | 0.32 | 0.3 |
| Mass density | ρ | [kg/m$^3$] | 112 | 1550 |

Table 2 - Stacking sequence for the different winglet regions.

| **External Upper (red)** | | | **Internal Upper (green)** | | | **External Lower (blue)** | | | **Internal Lower (yellow)** | | |
|---|---|---|---|---|---|---|---|---|---|---|---|
| Ply | θ | Material | Ply | θ | Material | Ply | θ | Material | Ply | θ | Material |

| | | | | | | | | | | | |
|---|---|---|---|---|---|---|---|---|---|---|---|
| 1 | 0° | Fiberglass | 1 | 0° | Fiberglass | 1 | 0° | Fiberglass | 1 | 0° | Fiberglass |
| 2 | ±45° | Fiberglass | 2 | | Foam | 2 | ±45° | Fiberglass | 2 | | Foam |
| 3 | ±45° | Fiberglass | 3 | ±45° | Fiberglass | 3 | ±45° | Fiberglass | 3 | ±45° | Fiberglass |
| 4 | ±45° | Fiberglass | 4 | ±45° | Fiberglass | 4 | ±45° | Fiberglass | 4 | ±45° | Fiberglass |
| 5 | 0° | Fiberglass | 5 | ±45° | Fiberglass | | | | 5 | 0° | Fiberglass |
| | | | 6 | 0° | Fiberglass | | | | | | |

Figure 2 - Distribution of material properties along the winglet.

### 2.2 Static test

In order to investigate the static behaviour of the winglet under the in-service bending loading conditions, an experimental test has been performed. The experimental set-up is shown in Figure 3. The winglet is fixed to a steel frame through 14 bolts, in view to reproduce the boundary condition of the winglet in its in service condition (fixed to the wing).

Figure 3 – Laser displacement measurement system [12].

In order to reproduce the maximum expected load acting on the winglet, which is equal to 300 N, an appropriate mass was used. In particular, the mass has been applied progressively from 1 kg up to the maximum load carried out by considering a mass of 28 kg. In this way, i.e., by applying progressively the load, it has been possible not only to plot the force-displacement curve, but also to verify the static behaviour of the winglet for each load. To reproduce the in service conditions, where the load is supposed to be like a distributed one, an ad-hoc load application wood frame was created in order to guarantee a uniformly distributed load. Its internal profile coincides with that corresponding of the winglet and its mass is equal to 0.1 kg, which is negligible if referred to the loading masses. The application load section was chosen according to the aerodynamic load distribution; therefore, the resultant pressure load is applied at 1/3 of the winglet length starting from its root. The application load axis is not perfectly perpendicular to the winglet, but it is inclined of 15°. The control point (shown in Figure 3), i.e. the displacement measurement point, is located at winglet tip in order to observe the maximum deformed shape.
The displacement was measured using a laser distance-meter LEICA DISTOTM A5. The laser, fixed to the steel winglet frame, was independent from the winglet displacements. In this way, the reliability of the proof was guaranteed. Furthermore, the laser was inclined with respect to the steel winglet frame of 15°; in this way, the laser and the winglet were perpendicular and the displacement measure is not affected by alignment errors.

### 2.3 Modal analysis

The determination of the modal parameters of the winglet was performed by using the so-called “roving hammer technique”. An ENDEVCO Modal Hammer 2302 was used to excite all the nodes of the experimental mesh and one accelerometer PCB 333B32 was used to measure the response at the corner node of the experimental mesh.
Since an impact test is not replicable (unless a mechanical device is used to hit the panel with the hammer), each measurement was obtained as the averaging spectrum of the responses of five different impacts, ensuring a coherence as much as possible close to the unity.
The experimental mesh is not constant along the structure and it consists of seventeen points. The data were recorded using the acquisition system LMS SCADAS III, in the bandwidth 0-512 Hz,

with a frequency resolution of 1 Hz, and, thus, analysed by means of the software LMS Test.Lab 16.a and Matlab tools. For each test, the free-free boundary conditions were applied: the winglet was suspended by using bungee cords in order to simulate free boundary conditions on all sides and, so, to validate the numerical model overcoming any problem arising from boundary conditions.

### 2.4 Guided wave propagation

The experimental tests campaign is widely described in [12]. Specifically, the equipment illustrated in Figure 4 consists of: a) a signal generator, which is connected to a piezoelectric (PZT) actuator; b) a set of twelve piezoelectric sensors usable as both actuating and receiving devices; c) an oscilloscope used to display the signals during the test and to acquire measurements; d) a home-made code for data post-processing.

Figure 4 - Experimental equipment for damage detection [12].

In order to limit the problem of the guided wave dispersion, strongly dependent on frequency, a narrow-band excitation has been preferred [15]. Specifically, the 4.5 sine tone-burst with Hanning window has been used as actuation signal. Two main tests have been performed with two excitation frequencies, 100 kHz and 200 kHz, respectively. In both experimental tests, guided waves are activated by transducer number 5. Once the signals were recorded (without filtering), a home-made Matlab code was used to post-process the data. Firstly, the experimental sensor signals have been shifted by a time lag, due to the amplifier. This time lag was estimated in 0.004 ms, a value close to that reported in [20]. Then, the ToF, i.e. the time needed for an emitted wave-packet to travel on the distance between two transducers, has been evaluated for each transducer path.
The ToF is the key feature used in the experimental-numerical results correlation. In order to reduce the dispersion phenomenon, the group velocity versus the measurement angles (referred to the sensors map and its reference system) was investigated varying the frequency in the range of 60 kHz - 200 kHz and the results are reported in [12].

## 3 Numerical investigations

The first step for the development of an efficient model able to simulate guided wave propagation is the numerical characterization of the medium which guided waves propagate through. For this reason the accuracy of the material characterization has been preliminary assessed by simulating the two preliminary experimental tests (the bending and the modal ones) and comparing their respective results.
Globally, three FE models have been developed. The first two, described in Section 3.1, concern the bending test and the modal analysis simulations; the third one, related to the simulation of guided wave propagation, is presented and discussed in the Section 3.2.
All the numerical analyses proposed in this paper have been developed and performed by using Abaqus®/CAE v. 6.14-1 software.
The results comparison of all the performed experimental tests and numerical simulations are given in Section 4.

### 3.1 FE model for static and modal analyses

The experimental bending static test was carried out by fixing the winglet to a steel frame through 14 bolts. In order to properly numerically reproduce such boundary condition, a good modelling

technique consists in fully constraining nodes corresponding to the areas covered by the bolted joints, so the holes and the steel fixture have not been modelled. Kinematic coupling constraints have been used to link the degrees of freedom of these nodes (slave nodes) to a common reference point (master node), as highlighted in Figure 5.a, which has been fully constrained. Concerning the loading condition, it has been modelled by reproducing the experimental configuration, as previously shown in Figure 3. The load has been applied at 1/3 of the winglet height starting from the root, on a shared reference point, by using, again, the kinematic coupling constraint approach (Figure 5.b). Finally, the gravity effect has been applied to the whole structure.

Figure 5 - Bolts (a) and load (b) boundary conditions.

Concerning the modal analysis there are not constraints and loading conditions to simulate, being a free-free oscillations problem, and the *Lanczos algorithm* has been defined as eigenvalues solver.

### 3.2 FE model for the guided wave propagation analysis.

In this section, a detailed description of the FE model used for the simulation of guided wave propagation in the winglet is proposed. Two different 4.5-cycle sine-burst actuation signals have been considered according to the experimental tests; the difference is related to the central frequency: 100 kHz and 200 kHz, respectively.
In particular, the modelling has been performed within an explicit environment since the wave propagation is a dynamic problem.
In a preliminary numerical investigation, two FE models based respectively on 2D and 3D finite elements have been developed in order to demonstrate the accuracy of the 2D finite elements in modelling guided waves propagation. Even if 2D finite elements seem to be not appropriate to model this phenomenon, several authors demonstrate their efficiency in terms of results accuracy and computational cost ratio [2, 15].
The average mesh size of both 2D and 3D FE models has been set to 0.5 mm (this choice is widely described in the following), providing a value of 30 NPW with a 100 kHz actuation signal. In order to compare the two FE techniques, a smaller area of the winglet has been investigated: the internal upper surface of the winglet (Figure 6), where the sensors are bonded on. This choice depends on the need to get the 3D model less time consuming.

Figure 6 – FE model of the internal upper surface.

Concerning the 3D model, C3D8R and C3D6 element types (from the Abaqus® elements' library) have been used . The former belongs to the hexahedral family, while the latter is a 6-node linear tetrahedral element; C3D6 finite elements have been used to discretize winglet areas characterized by a more complex geometry. Specifically, laminae have been modelled by means of 6 finite elements layers (one for each lamina). As a matter of the fact, 4971690 nodes and 4621064 elements, whose 4618544 are linear hexahedral elements (C3D8R type) and 2520 are linear tetrahedral elements (C3D6 type), have been used.
Regarding to the 2D FE model, it consists of 330076 shell elements and 331446 nodes. The laminate stacking sequence, in this case, has been modelled by means of 'composite shell section' tool, as implemented in the Abaqus software. It allows defining the number of integration points along the thickness, the orientation of the fibres and the material for each layer. 3 integration points for each lamina have been defined.
The results of the 2D and 3D FE models have been compared in Figure 7, providing a good agreement between the two techniques in terms of travel velocity and amplitudes.

By performing the two analyses by means of the same workstation (HP Z820) and under the same set-up conditions, it has been pointed out that the computational costs, evaluated in terms of elapsed time, consist of about 20 hours for the 3D FE model and about 2 hours for the 2D one.

Figure 7 –3D (blue dashed line) and 2D (green dashed line) FE models results comparison.

Concerning the characteristic length of the finite elements it has been set to an average size of 0.5 mm. Such value is carried out by a Matlab routine, which calculates the wavelength and consequently the mesh size providing a value of NPW of 30, when the actuation signal with central frequency of 100 kHz is considered. The choice of this NPW value depends on the need to address the developed FE model to future investigations on the interaction mechanisms between guided waves front and damages. A finer mesh is important to model properly damages. However, according to the performed convergence analysis, it must be noticed that, in the case of undamaged winglet, an average element size ranging between 2 mm and 0.5 mm (8 and 30 NPW respectively) provides an acceptable level of accuracy as well. Figure 8 shows the arrival time of the first wave packet measured for each transducer path versus the average finite element size. In details, three FE sizes have been investigated: 4 mm, 2 mm and 0.5 mm. As it can be seen from Figure 8, the numerical ToFs tend to the experimental ones as the mesh size decreases.

Figure 8 – Mesh convergence analysis.

NPW value also depends on the central frequency of the actuation signal. In fact, by considering the test case with central frequency of 200 kHz, the average mesh size of 0.5 mm provides a value of NPW of 15; as the frequency increases the wavelength decreases. A higher value of NPW is needed to model higher wave modes [15, 19]. From the literature, it has been found out that the recommended minimum NPW value to reproduce the first and second modes is 10 [15,19]; as in this work the attention has been focused on the first wave mode, then 15 NPW can be considered an acceptable value. By using an average mesh size higher than 0.5, it is not possible to investigate the guided wave propagation when excited by a 200 kHz actuation signal, since the NPW results to be lower than 10.

As a result of these investigations, the following analyses have been carried out by modelling the whole test article (Figure 9.a) by means of shell elements characterized by an average size of 0.5 mm. The developed FE model, shown in Figure 9.b, consists of 791111 shell elements and 792691 nodes. Such elements have been used to model the winglet skin. Three-dimensional brick elements have been used to model the sensors and the spar; 22880 nodes and 16005 elements, whose average length is 0.25 mm, for the sensors, and 347944 nodes and 326040 brick elements, whose average length is 0.5 mm, for the spar.

Figure 9 – Test case [12] (a) and FE model (b) of the investigated winglet with its boundary conditions.

The upper skin, as well as the lower one, is composed of two parts: the inner (green and yellow coloured area, respectively) and the outer (red and blue coloured area, respectively), as shown in Figure 9.b, which are different in lay-up and thickness. It has been fundamental to define properly, for each zone, the reference surface as offset from the shell mid-surface in order to guarantee the continuity of the geometry on the internal borders, as depicted in Figure 10, in which only a small part is reported.

Figure 10 - Zoom on the different thickness.

Furthermore, in order to model the composite laminates, the stacking sequence has been defined by means of "Composite Layout" tool, as implemented in the Abaqus® software; it allows defining the number of integration points through the thickness for each lamina. Each lamina has been modelled with three integration points. Orientation and material properties, shown in Table 1, are associated to these points.
Sensors have been numerically modelled in order to reproduce, as best as possible, the experimental ones in terms of both location (as shown in Figure 9.a) and material/geometry configurations. It is important to highlight that, in order to ensure the contact between sensors and skin, which have been meshed with different finite elements (brick and shell, respectively) and different sizes, the tie-constraint contact has been employed to link their degrees of freedom; a node-to-surface contact formulation has been considered. The adhesive layer between the sensors and the winglet has not been modelled. A consequence may be a slight divergence between the predicted signals and the experimental ones in terms of attenuation and delay of the signal.
Concerning the spar, it has been linked to the skin by merging the overlapped nodes, established that the skin and the spar have been meshed in a way to achieve the overlapping of the faced nodes.
The modelling of the actuation signal has been performed by applying radial displacements along the upper circumference of the actuator (Figure 11.a), equivalent to the experimental one, where the displacement value depend on applied voltage. The equivalent displacements can be achieved by means of [15]:

$$A(t) = \frac{1}{2} V \left[1 - \cos\left(\frac{2\pi t f_c}{n}\right)\right] \sin(2\pi t f_c) \qquad (1)$$

where, $A$ is the amplitude, t is the wave propagating duration, $f_c$ is the central frequency of the excitation signal, V is the maximum applied voltage and n is the number of cycles within the signal window (n=4.5). Figure 11.b shows the actuation signal and the equivalent displacement for the case with central frequency of 100 kHz.

Figure 11 - Radial equivalent displacements (a); actuation signal (blue line) [V] and equivalent radial displacements (red dashed line) [mm] (b).

As aforementioned, the experimental tests have been performed by considering the transducer in position "5" as actuator (Figure 9).
The validity of the results depends also on the critical time increment, which is the minimum time that an elastic wave takes to move across the smallest element in the model. It can be calculated as the ratio of the minimum distance of any two adjacent nodes to the maximum wave velocity. The explicit dynamic procedure solves every problem as a wave propagation problem; the solution can be obtained when the time increment is less than the critical time increment. Hence, it is important to estimate the critical time increment in order to set a reasonable time increment.
Finally, the winglet has been fully constrained at the root section, as highlighted in Figure 9.b.

## 4. Results and discussion

Results of each FE simulation have been compared with the experimental ones. Section 4.1 illustrates the results comparison for the bending test; Section 4.2 is related to the modal analysis; Section 4.3 is dedicated to the guided wave propagation.

### 4.1 Bending tests

Comparing the results for bending tests, the difference between the measured and predicted displacements (d) is lower than the 5%, under the applied mass, as it is possible to see in Figure 12. Figure 13 shows the contour plots of the displacements measured along the Y-direction of the reference system shown in Figure 13, carried out by considering a 1 kg mass.

Figure 12 – Numerical (red continuous line)-Experimental (blue dashed line) correlation: the static case.

Figure 13 – Measured displacement [mm] along Y-direction contour plot.

### 4.2 Modal analysis

The comparison of the first four vibrational modes is presented in Table 3. Since the first six modes correspond to rigid motion of the winglet, the modes reported in the Table 3 are the modes from 7 to 10. The contour plots related to such vibrational modes are shown in Figure 14.
Differences between the absolute value of predicted and experimental natural frequencies have been estimated to be lower than 10% , which can be considered as an acceptable agreement, established that the global stiffness of the parts involved in the vibrational modes refers to very complex geometrical and material configurations..

Table 3 - Experimental-numerical correlation: the first four natural frequencies.

| Mode # | Exp [Hz] | Num [Hz] | \|Deviation\| % |
|---|---|---|---|
| 1 | 36,739 | 36,746 | 0,019 |
| 2 | 41,928 | 46,466 | 9,712 |
| 3 | 66,819 | 67,358 | 0,82 |
| 4 | 76,949 | 70,57 | 8,29 |

Figure 14 – Measured contour plots from the 1$^{st}$ mode (a) to the 4$^{th}$ mode (d).

### 4.3 Guided wave tests

Numerical results, in terms of recorded signals, have been processed by means of a Matlab routine and then compared to respective experimental ones in order to assess the reliability of the developed predictive model. The most of the attention has been paid to the first waves packet, consisting of the symmetric-zero, $S_0$, mode. In the comparison process, the ToF feature, extracted by both numerical and experimental signals, has been used to evaluate the capability of the FE model.
The displacement field, shown at selected instants of time in Figure 15, illustrates the global displacement due to propagation of the wave in the examined winglet. In the first five frames, from (a) to (e), the wave propagation path vs time in the upper skin is illustrated, while the last one, (f), refers to the lower skin.

Figure 15 – Displacement field induced by the wave propagation at different step times.

Figure 16 shows the comparison between all simulated and experimental signals (except the signal recorded by sensor 1, which is not experimentally available) for the test case characterized by the actuation signal with central frequency of 100 kHz, activated by transducer 5. In particular, the signals achieved by sensors from 2 to 4 and from 6 to 12, respectively, are reported.

Each predicted signal is calculated as the average of the in-plane strains read by all nodes defining each sensor. Every single received signal has been post-processed by normalizing it respect to the absolute maximum among all signals. This value has been achieved in correspondence of sensor 6 in both numerical model and experimental tests.
The experimental signals have been shifted by a slight fixed time delay, the same for all of them, which may be caused by the amplifier, the experimental setup, the missing of damping factors in the FE model and, finally, by the fact that the adhesive between sensor and winglet has not been modelled. Nevertheless, the phase and the shape of the first modes match well for almost all the sensors.

Figure 16 – Numerical (blue continuous line) and experimental (red dashed line) comparison: actuation signal with central frequency of 100 kHz activated by sensor 5.

According to Figure 16, it can be noticed that as longer is the distance between the actuator and sensor, as more pronounced is the mismatch between numerical and experimental results in terms of signal amplitude. Such disagreement can be attributed, rather than the numerical errors which increase with the analysis time, to the missing damping factors in the FE model.
Analysing Figure 17, which represents the signal acquired by sensor 4 (red circled), the first wave mode $S_o$ and the scattered wave packet can be clearly identified. More in detail, the $S_0$ mode, which is the first waves packet recorded by sensor 4, has been linked to the contour plot representing the instant in which it reaches such sensor. Analogously, the second waves packet, recorded by the same sensor, representing the waves scattered by the boundary conditions, has been linked to the contour plot representing that instant.
Concerning the waves scattering phenomena, they are obviously expected on the right side of the winglet, in correspondence with the boundary edge. However, according to Figure 17, some scattered weaves can be also noticed on the left side. As guided waves reach the strong curvature on the left of the winglet, they should propagate underneath as if there were not edges. However, the strong curvature characterising this side reflects a part of the incident wave packet inducing boundary reflected waves, which amplitudes are lower if compared to the right edge scattered ones. Such assertion is motivated by the comparison of the scattered waves recorded by sensor 4 (Figure 17), placed nearby the winglet right edge, and the scattered waves recorded by sensor 6 (Figure 16), placed nearby the strong curvature. As a result, in terms of wave propagation, a strong curvature works as a boundary edge.

Figure 17 - $S_0$ mode propagation and scattered waves in the examined winglet.

According to Figure 16, it can be noticed an acceptable agreement between the predicted and the experimental signals. The slight mismatch between numerical and experimental results can be attributed, first of all, to the attenuation of guided waves with the distance (the level of attenuation can differ between experiments and numerical models). As aforementioned, no damping factors have been introduced in the material properties in order to save the computational costs.
In addition, the adhesive layer between sensors and winglet has been numerically modelled as a fully tied connection. So, the attenuation introduced by the glue has not been considered. According to the literature [2], the adhesive layer is usually omitted even if its thickness influences the amplitude of the signals.
Other factors contributing to the mismatch are: manufacturing defects, dispersion of the material properties, which may be different by the ones reported on the material technical specifications, and geometric tolerances such as thickness of the plate, position of the transducers, curvature, etc., that cannot be considered in the model.

In addition, the comparison of the numerical and experimental results of the analysis performed with the actuation signal characterized by central frequency of 200 kHz, activated by sensor 5, has been carried out and, for the sake of brevity, only the signal received by the sensor 4 is reported (Figure 18).

Figure 18 - Numerical (blue continuous line) and experimental (red dashed line) comparison: actuation signal with central frequency of 200 kHz activated by sensor 5 and received by sensor 4.

It has been previously underlined that the FE model used for the analysis at 200 kHz is characterized by only 15 NPW. However, a good level of accuracy has been achieved in this test case too.

## 5 Conclusions

The paper aims to provide a contribution on the modelling of Structural Health Monitoring systems for composite materials structures. In particular, the attention has been paid on the application of ultrasonic guided waves for damage detection purpose.

A FE model able to simulate the guided wave propagation in a real complex structural component made of GFRP has been developed. Most applications presented in literature focus mainly on coupons or simple structural components. In this work, a winglet for a general aviation aircraft has been investigated.

A preliminary investigation has been carried out to assess the numerical characterization of the materials properties by simulating two simpler conventional laboratory tests, such as the modal and the bending ones, previously conducted on the winglet by experiment. The numerical results are in good agreement with the experimental ones for both analyses.

A secondary numerical investigation has been dedicated to understand the best finite element technique for simulating guided wave propagation in a such complex composite structure. Specifically, the efficiency of shell and solid finite element types in modelling such kind of phenomenology has been measured in terms of predicted signals and computational costs. As a result, shell elements have been chosen thanks to their ability in simulating accurately the propagation mechanisms as well as reducing the computing time (reduced of about 90 % respect to 3D finite element based model). Also a mesh convergence analysis has been carried out to investigate the effects of shell element characteristic length. According to the performed convergence analysis, it has been found out that an average element size ranging between 2 mm and 0.5 mm (8 and 30 NPW respectively) provides an acceptable level of accuracy, measured in term of predicted time of flight.

Successively, the reliability of the FE model appointed to the propagation of the guided waves has been assessed by comparing the predicted signals, recorded in correspondence of 12 PZT sensors network arranged on to the model, with the experimental ones.

In particular, two 4.5-cycle sine-burst actuation signals with central frequencies of 100 kHz and 200 kHz have been considered. A good agreement between numerical and experimental results has been achieved for both analyses, performed at 100 kHz and 200 kHz, respectively.

Further investigations are planned by considering other excitation frequencies and actuator positions. In addition, also the introduction of one or more damages inside the winglet is going to be considered to assess the reliability of the model when damaged.

As a matter of fact, the presence of damage and defects alters the guided wave propagation; by comparing the received signals in the damaged winglet with the respective baseline signals (achieved in pristine winglet), it will be possible to understand the functionality of the guided wave based SHM system.

In conclusion, the development of an established and robust numerical model plays an important role in SHM systems applications. An experimental campaign is expensive and demanding, so, the numerical simulations can be considered mandatory to better understand some tricky aspects of the experimental wave propagation and to achieve great cost savings.

**Bibliography**

[1] Lamb H. On waves in an elastic plate. In: Proceedings of the Royal Society, 1917;93: 114-128.

[2] Schoch A. Seitliche Versetzung Eines Total Reflektierten Strahls bei Ultraschallwellen. Acustica 1952;2(1): 18-19.

[3] Frederick CL, Worlont DC. Ultrasonic thickness measurements with Lamb waves. Journal of Nondestructive Test1962;20: 51–55.

[4] Worlont DC. Experimental confirmation of Lamb waves at megacycle frequencies. Journal of Applied Physics 1961; 967-971.

[5] Rose JL. A vision of ultrasonic guided wave inspection potential. In: Proceedings of the Seventh ASME NDE Topical Conference 2001; NDE 20: 1–5.

[6] Su Z, Ye L, Lu Y. Guided lamb waves for identification of damage in composite structures: a review. Journal of Sound and Vibration 2006;295: 753–780.

[7] De Fenza A, Sorrentino A, Vitiello P. Application of Artificial Neural Networks and Probability Ellipse methods for damage detection using Lamb waves. Composite Structures, 2015;133: 390-403.

[8] Wang D, Ye L, Lua Y, Su Z. Probability of the presence of damage estimated from an active sensor network in a composite panel of multiple stiffeners. Composite Science and Technology 2009; 2054–2063.

[9] Sorrentino A, De Fenza A. Improved elliptical triangulation method for damage detection in composite material structures. Journal of Mechanical Engineering Science - Special Issue on SHM 2017;231(16): 3011-3023.

[10] Sorrentino A, De Fenza A. Damage detection in complex composite material structures by using elliptical triangulation method. In: the 11th International Workshop on Structural Health Monitoring, Stanford, California, USA, September 2017.

[11] Worden K, Manson G, Allman D. Experimental validation of a structural health monitoring methodology: part i. novelty detection on a laboratory structure. Journal of Sound and Vibration 2003;259: 323–343.

[12] De Fenza A, Petrone G, Pecora R, Barile M. Post-impact damage detection on a winglet structure realized in composite material. Composite Structures 2017;169: 129-137.

[13] Ciminello M, De Fenza A, Dimino I, Pecora R. Skin-spar failure detection of a composite winglet using FBG sensors. Archive of Mechanical Engineering 2017;64(3): 287-300.

[14] Ng CT, Veidt M, Rose LRF, Wang CH. Analytical and finite element prediction of Lamb wave scattering at delaminations in quasi-isotropic composite laminates. Journal of Sound and Vibration 2012;331: 4870–4883.

[15] Su Z, Ye L. Identification of Damage Using Lamb Waves. Applied and Computational Mechanics 2009. 48.

[16] Lee BC, Staszewski WJ. Modelling of Lamb waves for damage detection in metallic structures: part I – wave propagation. Smart Materials and Structures 2003;12: 804-814.

[17] De Luca A, Sharif-Khodaei Z, Aliabadi MH, Caputo F. Numerical Simulation of the Lamb Wave Propagation in Impacted CFRP. Procedia Engineering 2016;167: 109-115.

[18] De Luca A, Caputo F, Sharif Khodaei Z, Aliabadi MH. Damage characterization of composite plates under low velocity impact using ultrasonic guided waves. Composites Part B: Engineering 2018;138: 168-180.

[19] Kudela P, Zak A, Krawczuk M, Ostachowicz W. Modelling of wave propagation in composite plates using the time domain spectral element method. Journal of Sound and Vibration 2007;302: 728–745.

[20] Sharif-Khodaei Z, Aliabadi MH. Assessment of delay-and-sum algorithms for damage detection in aluminium and composite plates. Smart Materials and Structures 2014;23: 075007 (20pp).

[21] Yang C, Ye L, Su Z, Bannister M. Some aspects of numerical simulation for Lamb wave propagation in composite laminates Composite Structures 2006;75: 267–275.

[22] Hennings B, Lammering R. Material modeling for the simulation of quasi-continuous mode conversion during Lamb wave propagation in CFRP-layers. Composite Structures 2016;151: 142–148.

# Figure captions